Proceedings of
11th European Conference on Turbomachinery Fluid dynamics & Thermodynamics
ETC11, March 23-27, 2015, Madrid, Spain

ANALYSIS OF LOSSES IN CENTRIFUGAL PUMPS WITH LOW SPECIFIC SPEED WITH SMOOTH AND ROUGH WALLS

K. Juckelandt - S. Bleeck - F.-H. Wurm

University of Rostock, Faculty of Mechanical Engineering and Marine Technology, Institute of Turbomachines, Rostock, Germany, kay.juckelandt@uni-rostock.de

ABSTRACT

Numerical simulations (CFD) of industrial low specific speed pumps significantly differ from measurements. This keeps designers from using this method and rather sticking to prototyping. Experiments on a test pump with smooth walls are conducted. The influence of surface roughness on the performance is analyzed by applying micro-structured foils with realistic roughness to one side chamber. Surface roughness decreases the efficiency and needs to be considered in CFD simulations. Unsteady numerical simulations of the smooth pump are performed. A loss analysis reveals that most losses origin from volute and side chamber flow. Velocity profiles and pressure fields in these regions are in good agreement with experiments. Nevertheless, the predicted efficiency differs by 7 percent at overload. To validate rough wall models for pump simulations boundary layer measurements in a channel flow are carried out. Roughness effects on mean velocity and turbulent fluctuations are studied and applicability of wall-functions is evaluated.

D	Diameter	H	Pump head, channel height
L	Length	LDV	Laser Doppler Velocimetry
M	Torque	Opt	Best efficiency point
Q	Pump flow rate	SC	Side chamber
c_u	Circumferential velocity	n_q	Specific speed, $n_q = n \cdot \frac{\sqrt{Q}}{H^{3/4}}$
k_s	Equivalent sandgrain roughness height	Re_H	Reynolds-number: $Re_H = \frac{U_b H}{\nu}$
U_b	Bulk-velocity, $U_b = \frac{1}{\delta}\int_0^\delta \overline{U}(y)dy$	U_C	Free-stream velocity
u_τ	Frictional velocity, $u_\tau = \sqrt{\tau_w/\rho}$	δ	Boundary layer thickness at $U = 0.995 \cdot U_C$
η_i	Hydraulic efficiency, $\eta_i = \frac{\rho g Q H}{\omega M}$	Ψ	Pressure number, $\Psi = \frac{p_i - p_{SS}}{\frac{\rho}{2}\cdot\omega R_2}$
ω	Rotational velocity	$^+$	normalized with u_τ

INTRODUCTION

Numerical simulations are used for new and further development of turbomachinery to reduce development time and costs. This approach has established for many types of centrifugal pumps but it is subjected to errors for industrial pumps with low specific speed $n_q = 8 \ldots 15 min^{-1}$. Figure 1 shows a typical computed efficiency curve of an industrial pump. It is a common phenomenon that the simulated efficiency is determined too high and does not match the experimental characteristics. The reason for this deficit is not known so far. Subsequently, designers of this type of turbomachinery refrain from utilizing computational fluid dynamics (CFD) and stick to conventional prototyping.

Wang and Wang (2012) have focused on turbulence modeling in these pumps. They investigated eddy-viscosity models in stationary simulations with sliding-mesh-coupling. It was concluded that ω-based models yield better results than ϵ-based models. The efficiency could be reasonably captured at nominal load but still relative errors of $10 \ldots 16\%$ were reported in off-design operation. Effects of rotor-stator coupling were studied by Benigni et al. (2012). They carried out stationary frozen-rotor simulations and reported efficiency differences of 7 percentage points at overload. Transient rotor-stator simulations of an industrial pump were presented by Limbach et al. (2014). Their simulations

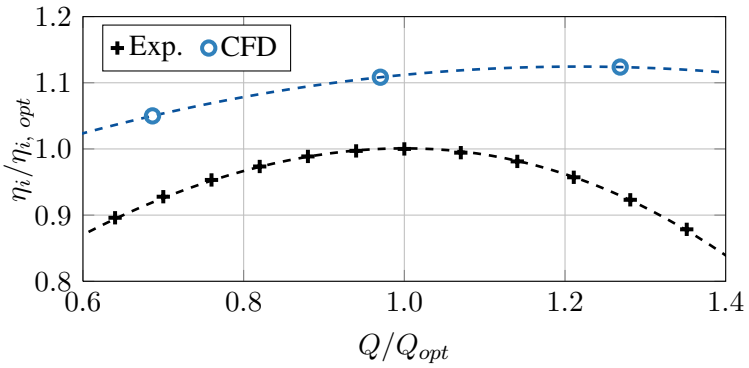

Figure 1: **Discrepancy between experiment and CFD of low specific speed industrial pump**

overestimated the efficiency and pump head at nominal load by 15 percentage points and 8.5% respectively. In these numerical studies no consideration has been given to surface roughness effects in of low specific speed pumps.

The impeller channels and side chambers of these pumps are long and narrow. Gülich (2010) reported that a significant fraction of losses origins from fluid friction that is dominant in the side chambers and the volute. Because most industrial pumps are sand casted, their surfaces presumably cause transitionally or fully rough behavior. Münch (1999) analyzed roughness effects experimentally and showed that typical surface roughness reduced the efficiency by 9 percentage points.

We have hypothesized that losses which are influenced by surface roughness might not be reproduced appropriately by numerical simulations that employ a wall-function approach (Juckelandt and Wurm (2013)).

In this research we investigate the performance of a test pump with smooth and rough walls. For the smooth wall setup we evaluate occurring losses and the applicability of numerical simulations for performance prediction. The influence of surface roughness on boundary layer flow was studied in a second experiment to validate rough wall treatment models in CFD codes for future simulations of low specific speed pumps.

EXPERIMENTAL SET-UP AND METHOD

Pump measurements

We built a test pump with $n_q = 13.4 min^{-1}$ in order to investigate the flow in a low specific speed and validate numerical simulations. Its modular design was adopted from an industrial pump with minor modifications for better experimental analysis (Fig. 2).

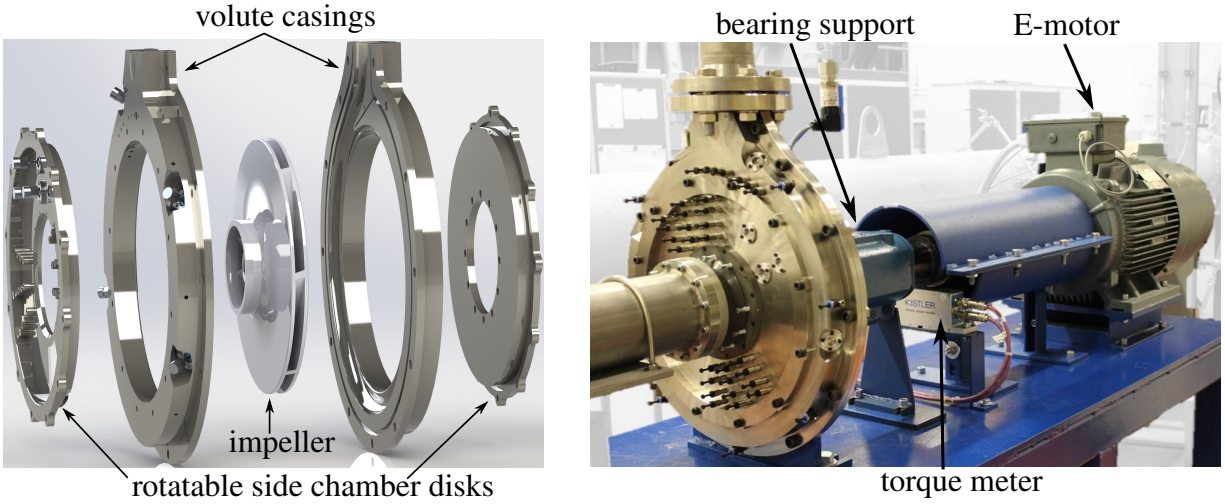

Figure 2: **Details of test pump**

All pump modules were manufactured by CNC milling to achieve high dimensional accuracy. Inner surfaces were polished to guarantee hydraulically smooth behavior ($R_a \leq 0.4\mu m$, $\frac{R_a}{\delta} \approx 2 \cdot 10^{-4}$). The surface topology of a corresponding industrial pump was reproduced to imitate realistically rough behavior. Therefore, the sand casted surfaces of the industrial pump were scanned with a three-dimensional scanning microscope. The spatial resolution was less than $1nm$ in z- and $1.5\mu m$ in x- and y-direction. After that transparent adhesive foils were structured with a high-power picosecond laser. The accuracy of this reproduction process depends on the processing speed and the optics used. In this work the accuracy was limited to $10\mu m$ in z- and $22\mu m$ in x- and y-direction for economic reasons. The equivalent sand grain roughness of the structured foils was estimated to be $k_s \approx 60\mu m$ $\left(\frac{k_s}{\delta} \approx 3 \cdot 10^{-2}\right)$.

The test pump was installed in a closed loop test rig and the inflow was straightened with a honey comb flow straightener $\left(\frac{L}{D} = 3.5\right)$ followed by an undisturbed tube section of $16D$. Flow rate was controlled with a control butterfly valve and the system pressure was adjusted to avoid cavitation.

Static pressure was measured at 61 pin-holes that are drilled in the volute entrance radius and in the side chamber disks. Both side chamber disks can be rotated, allowing a total of 267 different pressure measurement positions and spatially highly resolved measurements in the side chambers ($\Delta\alpha = 10°$). The pin-hole dimensions are $D = 0.5mm$ and $L = 1.0mm$. All pin-holes were connected to a collecting pipe with flexible tubes and were separately switched on with solenoid valves. In order to measure the pumps head accurately both suction- and pressure-side tubes were equipped with ring lines, each having 4 pin-holes. Pressure measurements were carried out using absolute pressure transmitters. Torque and rotational speed were measured with a non-contacting measuring flange that was installed between shaft and bearing. We determined the mechanical losses experimentally and corrected the measured torque data accordingly to obtain the torque of the impeller.

The side chamber disk at the suction side is equipped with an acrylic glass insert that provided optical access for non-intrusive velocity measurements with an one-dimensional LDV. The neodymium-YAG laser has a wavelength of $\lambda = 532nm$, $P = 300mW$ power and a focal length of $f = 250mm$. The focal volume dimensions are $0.17mm \times 3.0mm$ $(D \times L)$. The laser was aligned in axial direction and mounted on a traversing system that allows effective positioning with an accuracy of $0.8 \pm 0.5mm$. The LDV system was operated in back-scatter mode. At least 1000 validated bursts were sampled.

An uncertainty analysis for the experimental data was carried out. Systematic uncertainty of sensors used and stochastic uncertainty were evaluated. Gaussian uncertainty propagation was applied for indirect variables. The maximum measurement uncertainties U for of all pump results, were calculated with 95% confidence to be smaller than 1%, excluding Ψ ($U_\Psi = 4\%$).

Rough wall boundary layer flow

Surface roughness affects the boundary layer flow and significantly increases pressure losses. Validation data for later rough wall pump simulations were gathered by investigating roughness effects on a two-dimensional turbulent channel flow. The experimental investigations were performed in a closed loop test rig. Further details on the test rig are given by Turnow et al. (2012). Figure 3 shows

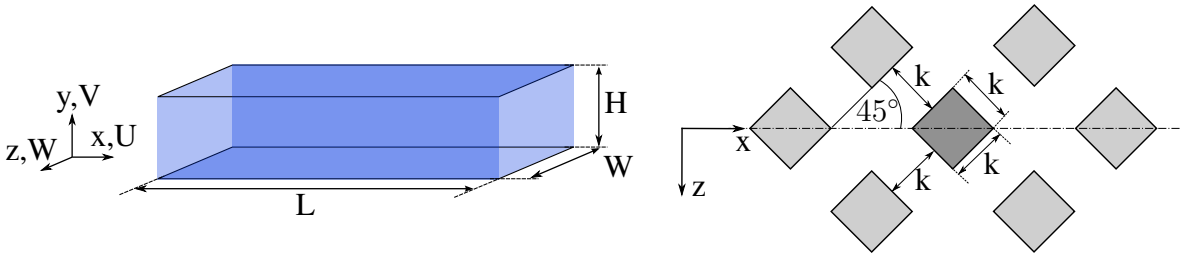

Figure 3: **Details of channel flow roughness geometry**

a sketch of the test section. The channel height H was $15mm$, its length ratio $L/H = 73.3$ and the aspect ratio $W/H = 13.3$. According to Dean (1978), two-dimensionality may be assumed for rectangular channels with aspect ratio $W/H > 7$. The Reynolds-number, based on channel height H and bulk-velocity U_b was $Re_H = 1.6 \ldots 1.8 \cdot 10^4$.

The channel was manufactured of transparent acrylic glass plates. The top and side walls were glued together, whereas the bottom plate could be changed. Artificial surface roughness was created by milling regular patterns of cubes in the bottom plates. The cubes with an edge length and pitch of k were skewed by $45°$ to the mean flow direction.

The flow rate was measured with an electromagnetic flowmeter. Density and viscosity of the fluid were derived from temperature and ambient pressure. Boundary layer measurements were carried out at $x = 50H$ using a vertically mounted two-dimensional LDV, operated in back-scatter mode. To increase coincidence the beams were rotated by $45°$, thus measuring components of U and W. In post-processing the true velocity vector was calculated by applying coordinate transformation. A coincidence interval of $\Delta t = 0.05ms$ for Doppler bursts of both channels was required for a valid signal. The focal volume dimensions are $0.146mm \times 2.4mm$ $(D \times L)$. The friction velocity u_τ was determined with the method of Clauser (1956), using log-law constants $\kappa = 0.41$ and $C = 5.2$.

COMPUTATIONAL METHODS

Unsteady RANS simulations of the pump were performed based on a three-dimensional finite volume method with the commercial solver ANSYS CFX 14.5. The conservation equations were solved with an implicit solver strategy using discretization schemes of second order accuracy. Transient rotor-stator coupling was used to account for interactions of the rotating impeller domain with stationary domains. The mesh of 8 million hexahedral-elements was created with ICEM CFD 15.0. All hydraulic components of the pump were considered with the following node distribution: volute: 2.3 million; each side chamber: 1 million; each impeller channel: 0.5 million and sealing gap, intake & piping: 1.1 million. Grid angles were larger than 27° and aspect ratios lower than 89 with a mesh expansion factor that was lower than 21. Boundary layers were modeled with a wall-function. The area averaged normalized wall distance of the first node was $\overline{y}^+ \approx 100$ at nominal load.

The k-ω-SST model from Menter (1994) was used for closure. We expect streamline curvature effects to influence the physics within pump flow. However, eddy-viscosity turbulence models cannot account for this effect a priori. Therefore, the curvature correction model of Smirnov and Menter (2009) was applied. It modifies the turbulence production term depending on the ratio of mean strain to vorticity tensor.

The following boundary conditions were used: relative static pressure was defined at the suction pipe inlet together with zero gradient turbulence. At the pressure pipe outlet a mass flow was given. All walls were assumed to be adiabatic, hydraulically smooth and the no-slip condition applied. The chosen time step equals a $3°$ rotation angle of the impeller, giving a RMS-Courant number of 6.5. A total of 8 revolutions was simulated with single-precision. Convergence was reached when the maximum residuals were smaller than $5 \cdot 10^{-3}$ and the monitored values had reached a steady state. Mean statistics were calculated during the last revolution.

RESULTS AND DISCUSSION

Influence of surface roughness on pump performance

The performance of centrifugal pumps at a given pump flow rate Q is evaluated in terms of pump head H, torque M and hydraulic efficiency η_i. The effective hydraulic power P_{hyd} of centrifugal pumps is decreased by losses that vary with flow rate. Typically, volumetric losses occur at part load and frictional losses prevail for higher flow rates. The fraction of frictional losses increases as the specific speed is reduced, due to larger impeller diameter. Furthermore, frictional losses are amplified

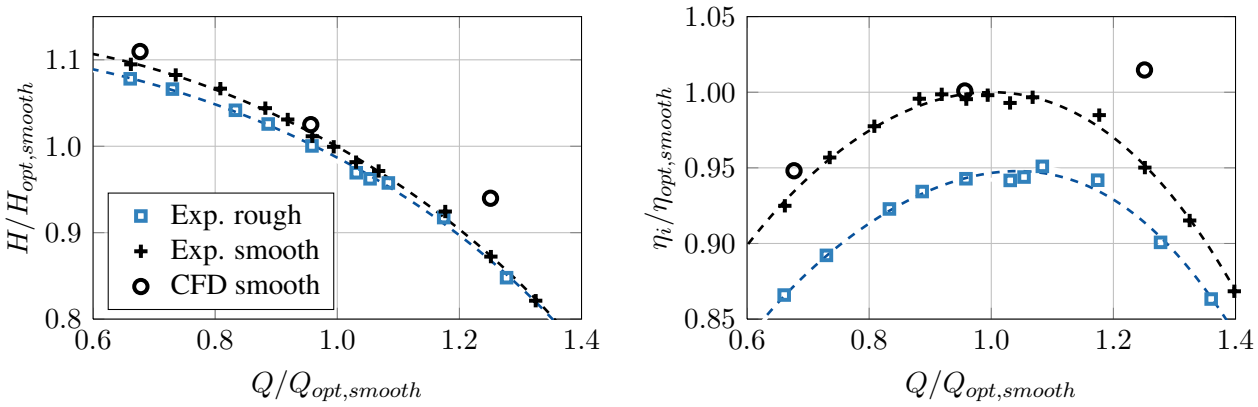

Figure 4: **Performance curves of test pump with variation of surface roughness**

by surfaces roughness. Mechanical power P_{mech} is derived from the torque that acts on the impeller's shaft. Normal and shear forces contribute to torque, while normal forces acting on the blades are dominant. We applied structured foils to the impeller and casing surfaces in the SS side chamber to analyze roughness effects. This modification did not alter the theoretical head of the pump.

Figure 4 shows the influence of rough side chamber surfaces on the performance. The pump head curves are depicted in the left diagram. The rough surfaces slightly increases pressure losses at low flow rates causing a difference of 1.5% at part load. We notice moderate sensitivity of this effect to flow rate as the additional pressure losses decrease at overload. This behavior typically indicates higher volumetric losses. We assume that the boundary layer thickness at the impeller has increased due to roughness. This could have increased the leakage flow rate and thereby volumetric losses that decrease the pump head. When walls are hydraulically smooth the pump head is well predicted by simulation at part and nominal load. Nevertheless, the CFD overestimates the pump head by 7.7% at overload, indicating that not all pressure losses were correctly captured.

Surface roughness effects on the pump's efficiency are shown on the right side of Fig. 4. The efficiency offset between smooth and rough walls is 5.3% at nominal load, which correspondents to 3.8 percentage points. Efficiency is further reduced by 6.9% at part load and by 4.2% at overload. The simulated efficiency shows good agreement with corresponding measurements at part and nominal load. Again, an over-prediction of 6.7% is evident at overload. Because the simulation matched the torque curve (not shown here) we assume that the discrepancy at overload is due to a phenomenon which is not primarily related to surface roughness.

Our results showed a characteristic similarity to the previously mentioned discrepancies of common pump simulations (see Fig. 1). The reported CFD curves have overestimated the efficiency over a large part of the operating range. Based on our results, we attribute this behavior to surface roughness effects. Therefore, we assume that a monotonic offset is caused by inappropriate modeling, or neglecting of roughness effects in numerical simulations of low specific speed pumps.

Pump flow with smooth walls

As a consequence of the discrepancies between smooth wall simulation and experiment at overload, we analyzed the flow field at nominal load and overload in an attempt to identify the cause.

Loss analysis

We sought more insight into the spatial loss distribution by analyzing the CFD results. Therefore, we calculated the losses in each computational domain by balancing power flows. Mechanical power $P_{mech} = M \cdot \omega$ is transferred to the fluid at rotating walls. At domain interfaces the transferred fluid power was calculated as $P_{in/out} = \frac{1}{\rho} \int p_{tot} d\dot{m}$. Hence, the difference between mechanical, incoming

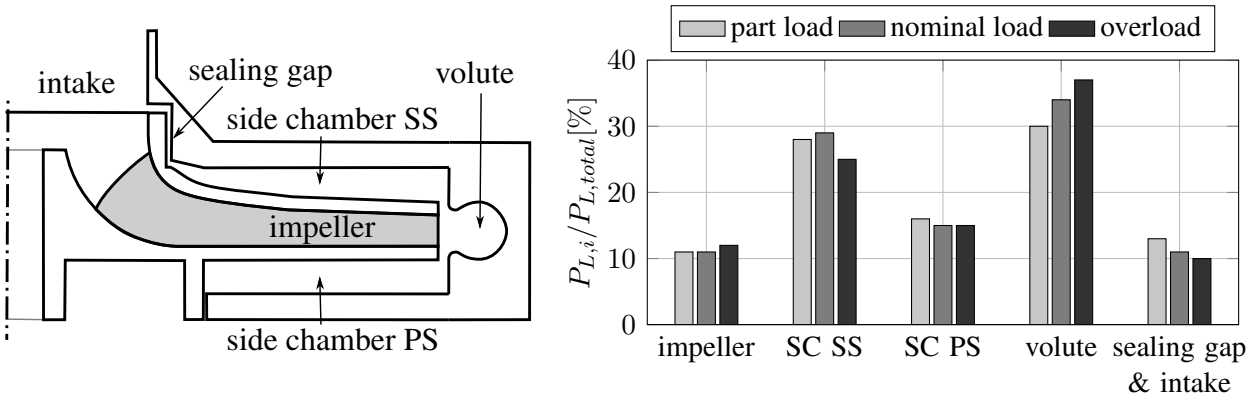

Figure 5: **Loss analysis by pump domain and flow rate**

and outgoing power yields in the power losses P_L per domain.

At off-design flow rate particularly strong secondary flows can arise that interact between multiple domains. For example, a vortex is induced in the intake section by increased leakage through the sealing gap at part load. However, the method used does not allow to assign losses to specific flow phenomena but to domains only. Because we cannot validate it with experimental data the results should rather be interpreted as qualitative trends.

Figure 5 shows the simulated loss distribution for different flow rates. The total of all losses increases with flow rate from Q/Q_{Opt}=0.66 to 1.22 by 27%. While the share of impeller and PS side chamber losses remains nearly constant, stronger flow rate dependency is detected in the other parts. At part load leakage through the sealing gap increases. A vortex in the suction pipe and impeller intake section results and losses increase. Volute flow losses are mainly caused by friction and increase with flow rate. The main share of losses originates from volute and SS side chamber flow in this pump. Both areas contribute to 63% of all losses at nominal load.

We focused our further analysis on side chamber and volute flow because most losses occur in these areas of the pump.

Side chamber flow

The predominant fluid motion in the side chambers is circumferential due to the impellers rotation. A radial pointing secondary flow is exerted by centrifugal force and leakage flow through the sealing gap. A variety of factors influences the velocity and pressure distribution in the side chambers: side chamber height, surface roughness, leakage flow, pressure distribution, volute flow interaction and rotational speed of the impeller (Gülich (2010)).

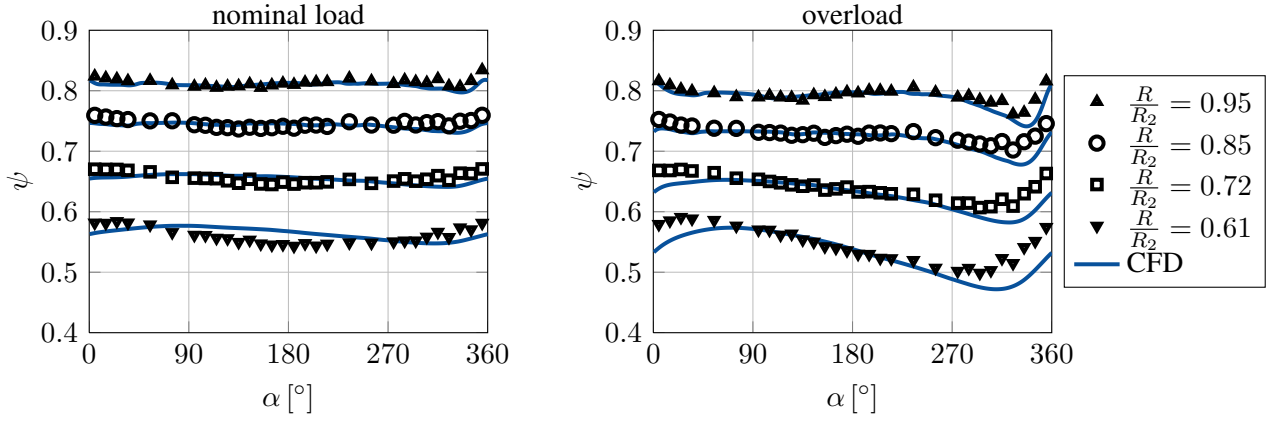

Figure 6: **Circumferential pressure profiles in side chamber at different radii**

Figure 6 presents the circumferential pressure distribution in SS side chamber on different radii. At nominal load the pressure level is highest at the outer radius and decreases in centripetal direction. The distribution is uniform near the impeller outlet but characteristics from volute flow are apparent (cmp. Fig. 8). Rotational symmetry is lost at the inner radius and a radial force follows pointing away from the tongue. There has not been reported a conclusive explanation for this phenomena. The numerical data accurately reproduces the pressure levels at all radii and captures the characteristics correctly. The simulated profile at the smallest radius is shifted counter-clockwise by $90°$.

At overload the pressure distribution is nonuniform near the impeller outlet and increasingly influenced by volute flow. The non-uniformity strongly increases in centripetal direction, causing radial forces to increase. The characteristics are reproduced qualitatively by CFD. However, the radial pressure drop is 4% higher and the simulated profile is shifted again in counter-clockwise direction.

Velocity measurements were performed in the SS side chamber near the tongue ($\alpha = -5°$) where strong volute interaction was shown and challenges for CFD are expected. The fluids motion is characterized by the ratio $k = \frac{c_u}{\omega R}$.

Figure 7 shows velocity profiles, with the distance from the impeller y is normalized by local side chamber height H. The flow is fully turbulent and a core region has developed. This can be derived from regions where $k = const.$. In centripetal direction the velocity ratio increases and the impeller is presumably accelerated by the flow for very small radii ($R/R_2 \leq 0.5$). Numerical results qualitatively match the measured profiles, but overestimate the circumferential velocity. Furthermore, differences of the boundary layer thickness are apparent. While the measured thickness at the impeller side is higher, the opposite is true at the casing wall. Even though uncertainties in the simulation cannot be ruled out completely, we attribute this difference to the velocity averaging procedure: tracer particles that cross the measurement volume are logged and an averaged value is calculated which corresponds to the focal point position. Because the length of the measurement volume is larger than the boundary layer thickness both fast and slow tracer particles are detected near a wall. Therefore, the resulting averaged velocity is too high.

Volute flow

Fluid from the impeller is collected in the volute. At nominal load it is assumed that $c_u \cdot R = const.$ is true. Hence, a uniform pressure distribution at constant radius R is expected. At overload the fluids circumferential velocity c_u is accelerated and the flow is prone to separation at the volute's tongue ($\alpha = 0°$) in the diffuser section. Gülich (2010) reported that friction and separation mainly contribute to pressure losses in the volute.

The pressure profile was measured at the volute entrance radius ($R = R_3$) and results are pre-

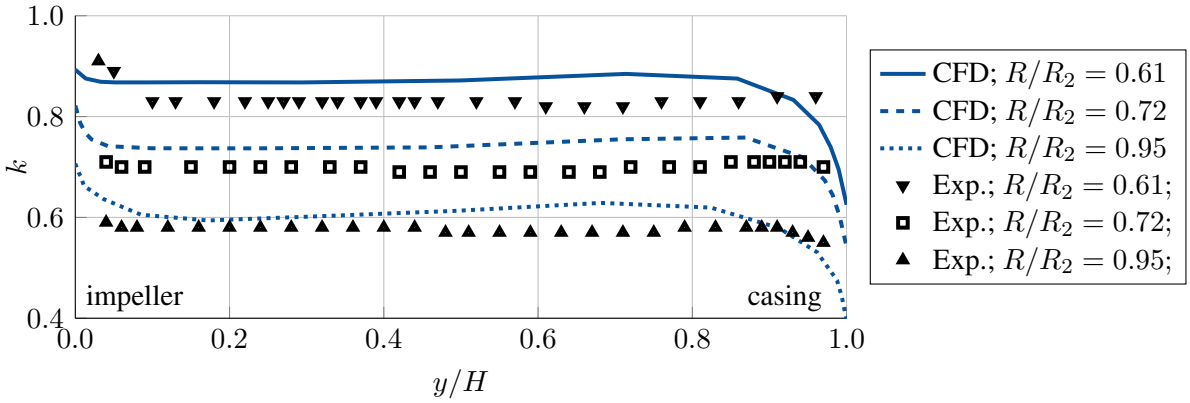

Figure 7: **Velocity distribution in SS side chamber at nominal load**

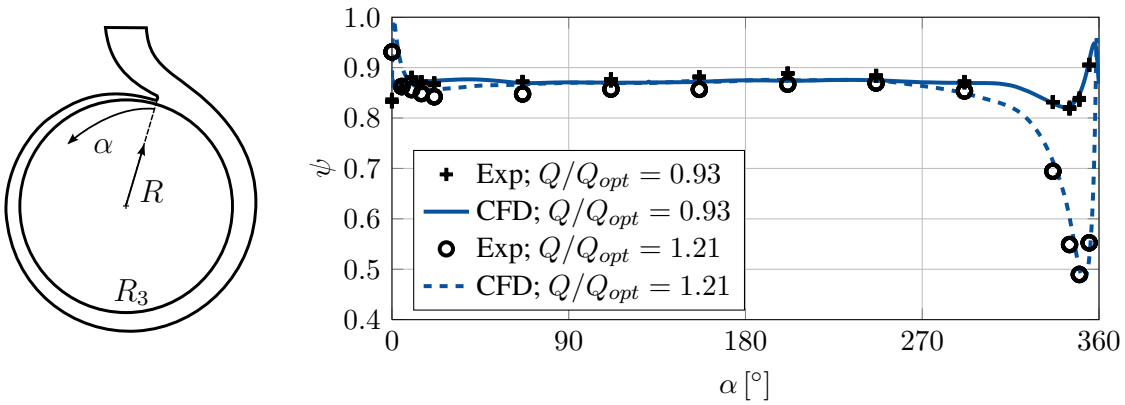

Figure 8: **Nomenclature and pressure profiles in the volute**

sented in Fig. 8. At nominal load the distribution is nearly uniform and disturbed near the volute's tongue only slightly. At overload flow rate the disturbance at the volute tongue is intensified and the above-mentioned flow acceleration can be deduced from a negative pressure gradient in circumferential direction ($\alpha = 270° \ldots 340°$). The characteristics were accurately captured by numerical simulations at both flow rates.

Influence of surface roughness on turbulent boundary layer

We pointed out that surface roughness significantly contributes to losses in low specific speed pumps. Hence, it is necessary to model this effect on boundary layer flow in numerical simulations in an appropriate way. Roughness effects are often modeled with wall-functions that determine the mean velocity and turbulence based on empirical formulas. In order to evaluate the applicability of such models we carried out experiments on a two-dimensional turbulent channel flow with rough walls.

In wall bounded flows momentum exchange takes place in the boundary layer due to shear. Surface roughness enhances momentum exchange due to higher wall shear stress and thus causes higher losses. Streamwise fluctuations mainly contribute to turbulence in this test case. According to Townsend (1976) the influence of roughness is limited to $y = 3 \ldots 5\ k_s$ within the boundary layer (rough sublayer) and the mean velocity profiles of smooth and rough wall flows collapse in defect form $\frac{U_C - U(y)}{u_\tau} = f\left(\frac{y}{\delta}\right)$. This hypothesis allows to make use of rough wall models in CFD that are based on smooth wall similarity, such as the wall-function approach. For similarity to exist in the outer layer of the boundary layer, Connelly et al. (2006) reported that sand grain roughness k_s should be small compared to boundary layer thickness ($\delta/k_s \geq 6$).

In this work boundary layer similarity was tested on two types of three-dimensional rough surfaces. Table 1 summarizes key parameters:

Table 1: **Surface roughness parameter**

	$k\ [mm]$	k_s^+	δ/k	δ/k_s
roughness #1	0.6	29	16	24
roughness #2	2.0	125	5	8

When the mean velocity profile is scaled with inner variables (u_τ) a down- and rightward shift of the mean velocity profile can be seen for rough surfaces as wall shear stress τ_w increases (Fig. 9). As the magnitude of this shift depends on the roughness scale k_s, it is commonly utilized for wall-function approaches. In defect form all profiles collapse away from the wall, indicating similarity. Near the wall both rough surfaces show a smaller velocity defect and roughness #2 additionally deviates

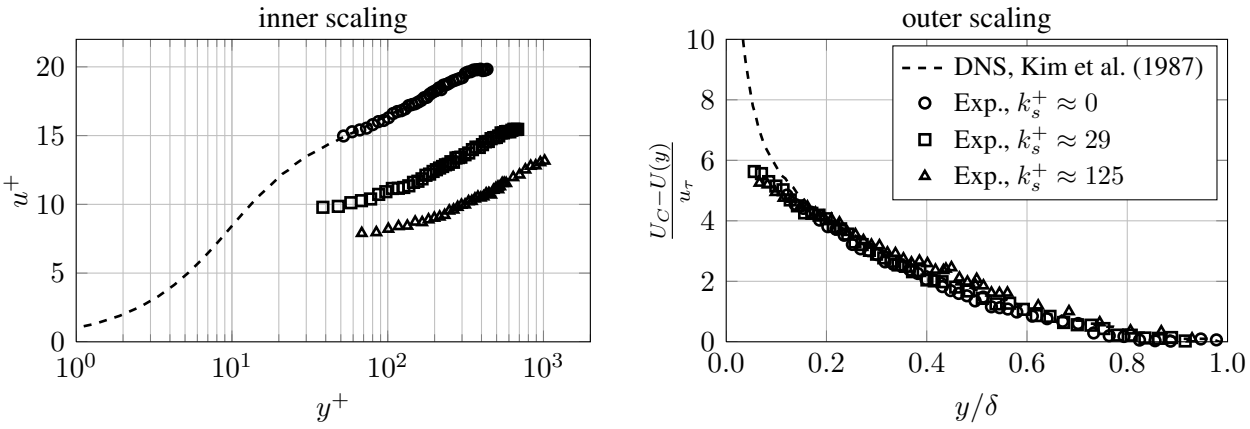

Figure 9: **Mean velocity scaling for smooth and rough surfaces**

between $0.4 \leq \frac{y}{\delta} \leq 0.6$. This perturbation results from direct roughness effects as the rough sublayer extends to $\frac{y}{\delta} \approx 0.6$.

Experimental results of turbulence profiles are depicted in Fig. 10. Streamwise fluctuations in smooth wall boundary layer flow show a peak at $y^+ \approx 15$ because of viscous effects. Instead of exerting a near wall rise, rough walls show a plateau in the outer-, resp. log-layer as viscous effects vanish. The same profiles are plotted in outer scaling to check for similarity. Once more, smooth wall and roughness #1 profiles collapse. Perturbations extend well beyond the rough sublayer which is marked with a dash dotted line for roughness #2.

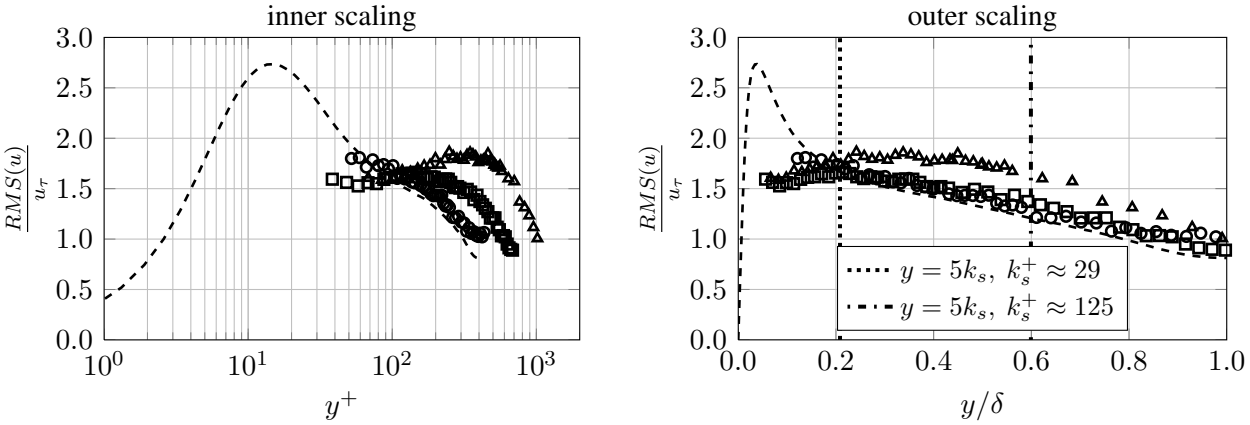

Figure 10: **Scaling of streamwise velocity fluctuations for smooth and rough surfaces**

CONCLUSIONS

Significant differences between measured and simulated efficiency were reported for low specific speed pumps and have precluded the use of CFD methods in the past. This paper evaluated occurring losses and the applicability of numerical simulations for performance prediction for this type of centrifugal pumps.

We have scrutinized surface roughness effects on the pump performance experimentally. The efficiency was decreased due to surface roughness. Therefore, we conclude that the assumption of hydraulically smooth walls in simulations of industrial pumps is invalid.

Transient simulations of a complete three-dimensional pump model were carried out. Experiments were conducted to obtain the flow field and performance data of a test pump with hydraulically smooth walls. The simulated and measured flow fields were in reasonable agreement at all flow rates and yet the simulated efficiency was too high at overload. Possibly losses were not reproduced correctly and

we assume that they occur downstream the last measurement position. We will examine this aspect in further research.

Simulations of surface roughness commonly utilize a modified wall-function method to determine mean velocity and turbulence. This approach relies on a similarity hypothesis between smooth and rough wall flows. We studied the influence of surface roughness on a boundary layer flow to evaluate the applicability of the wall-function method. Similarity of mean velocity and turbulent fluctuations were confirmed for large ratios of boundary layer thickness to roughness. Differences were observed when the roughness was too large. In this case the similarity hypothesis is violated and wall-functions should not be used. Additional studies will be necessary to evaluate the wall-function applicability in simulations of low specific speed pumps.

ACKNOWLEDGEMENTS

This work is financially supported by the AiF in the framework of Industrial Collective Research (IGF, project 17740 BR/1), supported by Federal Ministry for Economic Affairs and Energy on the basis of a decision by the German Bundestag.

References

Benigni, H., Jaberg, H., Yeung, H., Salisbury, T., Berry, O., and Collins, T. (2012). Numerical simulation of low specific speed american petroleum institute pumpes in part-load operation and comparison with test rig results. *Journal of Fluids Engineering*, 134(024501).

Clauser, F. H. (1956). The turbulent boundary layer. *Advances in Applied Mechanics*, 4:1–51.

Connelly, J. S., Schultz, M. P., and Flack, K. A. (2006). Velocity-defect scaling for turbulent boundary layers with a range of relative roughness. *Experiments in Fluids*, 40(2):188–195.

Dean, R. B. (1978). Reynolds number dependence of skin friction and other bulk flow variables in two-dimensional rectangular duct flow. *Journal of Fluids Engineering*, 100:215–223.

Gülich, J. F. (2010). *Kreiselpumpen: Handbuch für Entwicklung, Anlagenplanung und Betrieb*. Springer Berlin, Heidelberg, Berlin and Heidelberg, 3 edition.

Juckelandt, K. and Wurm, F.-H. (2013). Modellierung und Simulation der Strömung in Pumpen kleiner spezifischer Drehzahl: Final Report for VDMA & FFP.

Kim, J., Moin, P., and Moser, R. D. (1987). Turbulence statistics in fully developed channel flow at low reynolds number. *Journal of Fluid Mechanics*, 177:133–466.

Limbach, P., Kimoto, M., Deimel, C., and Skoda, R. (2014). Numerical 3d simulation of the cavitating flow in a centrifugal pump with low specific speed and evaluation of the suction head. *Proceedings of ASME Turbo Expo 2014*, pages 1–9.

Menter, F. R. (1994). Two-equation eddy-viscosity turbulence models for engineering applications. *AIAA Journal*, 32(8):1598–1605.

Münch, A. (1999). *Untersuchung zum Wirkungsgradpotential von Kreiselpumpen*. PhD thesis, TU Darmstadt, Darmstadt.

Smirnov, P. E. and Menter, F. R. (2009). Sensitization of the sst turbulence model to rotation and curvature by applying the spalart–shur correction term. *Journal of Turbomachinery*, 131(4).

Townsend, A. A. (1976). *The structure of turbulent shear flow*. Univ. Pr., Cambridge, 2. ed., 1. pbk. ed. edition.

Turnow, J., Kornev, N., Zhdanov, V., and Hassel, E. (2012). Flow structures and heat transfer on dimples in a staggered arrangement. *International Journal of Heat and Fluid Flow*, 35:168–175.

Wang, Y. and Wang, W. J. (2012). Applicability of eddy viscosity turbulence models in low specific speed centrifugal pump. *IOP Conference Series: Earth and Environmental Science*, 15(6):062013.